Numerical stability analysis of an acceleration scheme for step size constrained time integrators

Vandekerckhove, Christophe; Roose, Dirk; Lust, Kurt

Published in:
Journal of Computational and Applied Mathematics

DOI:
10.1016/j.cam.2006.01.029

Available online at www.sciencedirect.com
ScienceDirect
Journal of Computational and Applied Mathematics 200 (2007) 761–777
JOURNAL OF COMPUTATIONAL AND APPLIED MATHEMATICS
www.elsevier.com/locate/cam

Numerical stability analysis of an acceleration scheme for step size constrained time integrators

Christophe Vandekerckhove[a,*], Dirk Roose[a], Kurt Lust[b]

[a] *Department of Computer Science, K.U. Leuven, B-3001 Heverlee, Belgium*
[b] *Institute of Mathematics and Computing Science, University of Groningen, 9700 AV Groningen, The Netherlands*

Received 4 April 2005; received in revised form 18 October 2005

Abstract

Time integration schemes with a fixed time step, much smaller than the dominant slow time scales of the dynamics of the system, arise in the context of stiff ordinary differential equations or in multiscale computations, where a microscopic time-stepper is used to compute macroscopic behaviour. We discuss a method to accelerate such a time integrator by using extrapolation. This method extends the scheme developed by Sommeijer [Increasing the real stability boundary of explicit methods, Comput. Math. Appl. 19(6) (1990) 37–49], and uses similar ideas as the projective integration method. We analyse the stability properties of the method, and we illustrate its performance for a convection–diffusion problem.

MSC: 37M05; 65L20

Keywords: Stability analysis; Time integration

1. Introduction

In this paper, we consider discrete evolution equations of the form

$$y_{n+1} = \Phi_{\Delta t}(y_n), \quad y_n \in \mathbb{R}^N, \tag{1}$$

where $\Phi_{\Delta t}$ is a continuous and differentiable map, y_n the state at time t_n and y_{n+1} the state at time $t_{n+1} = t_n + \Delta t$. We assume that the map (1) generates a sequence of points $\{y_i\}_{\Delta t}$ along a trajectory of a—not necessarily known—time-continuous evolution equation. Therefore, (1) is sometimes also called a time-stepper. Furthermore, we assume that the time step Δt is fixed and small compared to the time scales of the dynamics of interest. Hence, iterating on (1) to compute the sequence $\{y_i\}_{\Delta t}$ is not very efficient, as the solution could also be described sufficiently accurate by another sequence $\{\overline{y}_j\}_{\Delta T}$, where the time step between the successive states is $\Delta T \gg \Delta t$. In this paper, we shall study a simple scheme that efficiently computes such a new sequence $\{\overline{y}_j\}_{\Delta T}$, based only on iterations of the map (1) and an extrapolation method.

* Corresponding author. Tel.: +3216327082; fax: +3216327996.
E-mail address: christophe.vandekerckhove@cs.kuleuven.be (C. Vandekerckhove).

0377-0427/$ - see front matter © 2006 Elsevier B.V. All rights reserved.
doi:10.1016/j.cam.2006.01.029

Perhaps the most typical example of a discrete system of the form (1) with time steps that are smaller than required by accuracy, is that of an explicitly discretised parabolic partial differential equation (PDE). When adopting the method of lines approach, the spatial discretisation yields a large, stiff system of ordinary differential equations (ODEs), and the time step of an explicit ODE solver will be small for stability reasons. Several techniques were proposed in this context to obtain explicit schemes with larger step sizes. Among them are the Chebyshev methods (also called stabilised methods), which are explicit Runge–Kutta (RK) methods with extended stability domains along the negative real axis [10,7,1]. However, these methods make explicit use of the PDE equations, while we want to develop a method that can accelerate a discrete time integrator (1), independent of the underlying model or equations. The time-stepper could be an explicit PDE solver, but it could as well be another simulation code, such as a lattice-Boltzmann code. This "black box" strategy is particularly interesting when the time-stepper is a legacy code that represents many man-years of development, and that cannot be altered in an easy manner. Our main motivation (and inspiration) however to study schemes for the acceleration of (1) is the development of efficient methods for multiscale problems.

Often, one is only interested in the deterministic macroscopic behaviour of the system, while the underlying processes at the microscopic level are heterogeneous or stochastic in nature. Traditionally, studying the long-term dynamics of multiscale processes involves the explicit derivation of a set of macroscopic equations. Recently, Kevrekidis et al. developed a framework to compute the evolution of the macroscopic variables which circumvents the explicit derivation of the macroscopic equations [6,4]. The main tool for this is called the coarse-grained time-stepper, which is a map from the macroscopic variables at time t_n to those at time $t_n + \delta t$. This map is obtained through the time evolution of appropriately initialised microscopic simulations. The time step δt is larger than the microscopic time scales but smaller than the macroscopic time scales. An efficient scheme is obtained by combining the coarse-grained integrator with the projective integration method (PIM) of Gear and Kevrekidis, which uses a suitable extrapolation technique to predict a future macroscopic state [6,4]. In this way, one can restrict the microscopic simulations to only small time intervals.

The projective integration idea was adopted and analysed first in the context of stiff ODEs with the eigenvalues clustered into two regions along the real axis [2]. A projective integration step uses first a stable explicit integrator (called the "inner integrator") to compute a number of points with a very small time step (we shall refer to this as a "group of inner steps"). Then, based on the last points of this group of inner steps, a polynomial extrapolation is used to approximate the solution far ahead. The inner integration steps also serve to damp the fast components excited in the previous extrapolation step and thus retain stability. A linear stability analysis of this process was done in terms of the eigenvalues of the inner integrator. In this way, the analysis is fully decoupled from the details of the inner integrator. It was shown that the parameters in the projective integration scheme can be chosen such that the method is absolutely stable if the eigenvalues are indeed clustered in two regions. Furthermore, it was shown that one can project over large steps, and thus gain dramatically in efficiency. If the problem at hand does not have such a clustered eigenvalue spectrum, the acceleration that can be obtained is rather limited. In [3], one applies the projective integration idea in a recursive manner. The projective integrator can be viewed as just another time-stepper, which can be used in a further projective integrator, and so on. These recursive methods are called telescopic projective integration methods (TPIMs). It was shown that by introducing these levels of recursion, one can achieve very large accelerations, even if there is a large spread of eigenvalues with no gaps in their spectrum.

In this paper, we will analyse a scheme that is very similar to the PIM as described in [2], but which uses a polynomial extrapolation method based on N points that come from N different groups of inner steps, instead of only from the last group. In this way, we obtain a multistep scheme. We will show that this scheme has other stability properties, which may be beneficial for certain types of problems. We also expect that this scheme might be useful if the time-stepper is stochastic in nature, such as a Monte Carlo simulation. The scheme can then be applied without modifications as long as we take a large number of integration steps in each group of inner steps.

It should be noticed that the idea of extrapolating known states to predict a future state was already developed by Sommeijer at the end of the 1980s in the context of overcoming the step size restriction for parabolic PDEs [9]. Based on the simplest well-known explicit integration rules (e.g. RK schemes), new schemes were constructed which allow for considerably larger time steps (i.e., the RK scheme is adapted to a new scheme with a larger stability boundary). The accuracy and the linear (real) stability were analysed for some of these schemes. The schemes considered in this paper can be seen as an extension of the class of schemes in [9].

The outline of the paper is as follows. In Section 2 we will first describe the method, introduce some notation and reiterate on the differences between the PIM proposed by Gear and the method we consider in this paper. In

Section 3 we extensively analyse the linear stability properties of the method, in a similar decoupled fashion as in [2]. These theoretical results are validated by some numerical experiments for a simple model problem in Section 4. Finally, in Section 5 we give a brief discussion and summarise the main conclusions of this paper.

2. Description of the method

We now show how the sequence $\{\overline{y}_j\}_{\Delta T}$ can be computed. Suppose that we already know $\{\overline{y}_0, \overline{y}_1, \ldots, \overline{y}_j, \ldots, \overline{y}_n\}$ at times $T_j = j\Delta T$. Then the computation of $\overline{y}_{n+1}$ at $T_{n+1} = (n+1)\Delta T$ consists of two steps. First, the value at time $T_{n+1} - k\Delta t$ (for some $k \in \mathbb{N}$) is determined by extrapolation using the Nth-degree polynomial P_N interpolating in $\overline{y}_{n-N}, \overline{y}_{n-N+1}, \ldots, \overline{y}_n$. From this point, we then do k time steps with (1) to obtain $\overline{y}_{n+1}$ at time T_{n+1}. It is clear that the overall efficiency is increased as long as the stability is maintained. However, we expect to lose some accuracy because of the extrapolation.

Let m be defined such that

$$(m+k)\Delta t = \Delta T.$$

Note that m does not have to be an integer. The fraction of ΔT that was bridged by the extrapolation method is thus

$$\mu := \frac{m}{m+k},$$

and if the overhead due to the extrapolation is negligible, a speedup

$$S \approx \frac{m+k}{k} = 1 + \frac{m}{k} = \frac{1}{1-\mu}$$

is obtained.

The procedure is summarised in Algorithm 1. The values of $\overline{y}_i{}^*$ should be considered as an intermediate result only.

Algorithm 1 Computation of the sequence $\{\overline{y}_j\}_{\Delta T}$

Required: $\overline{y}_{n-N}, \overline{y}_{n-N+1}, \ldots, \overline{y}_n$
Determine $l_s = \frac{\mu\cdot(\mu+1)\cdots(\mu+N)}{(s)!(N-s)!(-1)^s(\mu+s)}$, $s = 0, \ldots, N$.
$t = n$
repeat
$t = t + 1$
$\overline{y}_t^* = \sum_{s=0}^{N} l_s \cdot \overline{y}_{t-1-s}$
$\overline{y}_t = \Phi^k(\overline{y}_t^*)$
until $t\Delta T \geqslant T_{\text{end}}$

A schematic picture of the method is shown in Fig. 1. In the same figure we also illustrate the PIM and the TPIM. Note that the meaning of k in this paper differs slightly from the meaning of k used in [2,3]. Fig. 1 clearly shows that Algorithm 1 is a multistep method. To compute $\overline{y}_1$, we had to integrate using (1) over the whole time interval. The PIM and TPIM on the other hand are one-step methods. In [8], the PIM was extended to an Adams–Bashforth-like multistep scheme. In [4], the extrapolation points of the PIM are chosen further apart, but all of them still belong to the last group of inner steps. Algorithm 1 can be seen as a further extension of this idea, where we now use points from different group of inner steps.

3. Stability analysis of the scheme

In this section we will study the stability properties of Algorithm 1. Rather than starting the analysis from the traditional linear test equation, we start from the scalar linear "test integrator"

$$y_{i+1} = \Phi_{\Delta t}(y_i) = \rho y_i, \quad y_n \in \mathbb{R}.$$

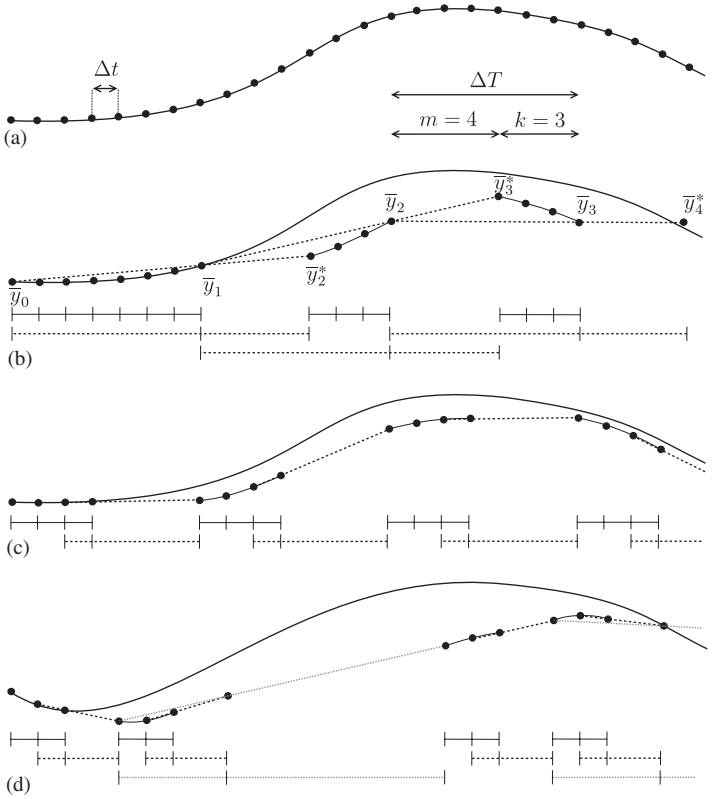

Fig. 1. A schematic comparison of unaccelerated time-stepping (a), and accelerating the time-stepper using Algorithm 1 (b), PIM (c) or TPIM (d). All methods are based on linear extrapolation. In (b) and (c) we used $k = 3$ and $m = 4$. In (d) we chose $k = m = 2$ and we added one extra level of recursion.

If $|\rho| < 1$, then $\lim_{i\to\infty} y_i = 0$, and we want this property to be preserved by the accelerated scheme. When applying our scheme to this test integrator, we get

$$\overline{y}_{j+1} = \Phi^k_{\Delta t}(\overline{y}^*_{j+1}) = \rho^k \overline{y}^*_{j+1} = \rho^k \sum_{s=0}^{N} l_s \cdot \overline{y}_{j-s},$$

where

$$l_s = \frac{\mu \cdot (\mu+1) \cdots (\mu+N)}{(s)!(N-s)!(-1)^s(\mu+s)}.$$

This sequence tends to zero as j goes to infinity for any set of starting values $y_{-N}, \ldots, y_0$ and given values of ρ, k, μ and N if all zeroes of the characteristic equation

$$P(\xi, \rho, k, \mu, N) \equiv \xi^{N+1} - \rho^k \sum_{s=0}^{N} l_s \cdot \xi^{N-s} = 0 \tag{2}$$

lie inside the unit circle. The stability region $\Omega_N(k, m)$ is then defined as

$$\Omega_N(k, m) = \{\rho | P(\xi, \rho, k, \mu, N) = 0 \Rightarrow |\xi| < 1\},$$

i.e., the set of all values of ρ for which all roots of $P(\xi, \rho, k, \mu, N)$ lie inside the unit circle.

Property 1. *$\Omega_N(k, m)$ is D_k-symmetric, with D_k the symmetry group of the regular k-gon with vertices* $e^{i2\pi j/k}$, $j = 0, \ldots, k-1$.

Proof. It is sufficient to prove that $\Omega_N(k, m)$ is invariant under reflection about the real axis and rotation over an angle $2\pi/k$, since these transformations generate the symmetry group [5]. The invariance under reflection holds since the roots of $P(\xi, \overline{\rho}, k, \mu, N) = 0$ are the complex conjugates of the roots of $P(\xi, \rho, k, \mu, N) = 0$. The rotational invariance holds since $P(\xi, \rho e^{i2\pi/k}, k, \mu, N) = P(\xi, \rho, k, \mu, N)$. □

Because of these symmetries, it is sufficient to study the stability region in the sector

$$R = \left\{ z \in \mathbb{C} | 0 \leqslant \arg z \leqslant \frac{\pi}{k} \right\}$$

of the complex plane. The remainder of the stability region can then be obtained by reflections and rotations. We will now study the stability region for linear extrapolation ($N = 1$) and quadratic extrapolation ($N = 2$) in more detail.

3.1. Stability analysis of the scheme with linear extrapolation

In this case, the stability polynomial (2) reduces to

$$P(\xi, \rho, k, \mu, 1) = \xi^2 - (1 + \mu)\rho^k \xi + \mu\rho^k = 0. \tag{3}$$

Hence the stability domain is bounded by the curve $\rho(\theta)$ implicitly defined by

$$P(e^{i\theta}, \rho(\theta), k, \mu, 1) = 0. \tag{4}$$

From (3) and (4) we get

$$\rho(\theta, k, \mu) = \sqrt[k]{\frac{e^{i2\theta}}{(1 + \mu)e^{i\theta} - \mu}}, \tag{5}$$

where we still need to choose $\arg \rho$ if $k > 1$. It is possible to show that $\mathrm{Im}(\rho(\theta, 1, \mu)) > 0$ if $\theta \in (0, \pi)$, and for symmetry reasons, $\mathrm{Im}(\rho(\theta, 1, \mu)) < 0$ if $\theta \in (-\pi, 0)$. Moreover, $\rho(\theta, 1, \mu)$ is a continuous function of θ. Therefore, the choice

$$\arg \rho \in [(2l - 1)\pi/k, (2l + 1)\pi/k) \quad \text{if } \theta \in [(2l - 1)\pi, (2l + 1)\pi) \tag{6}$$

in (5) results in a continuous explicit parameterisation. The curves for various values of k and μ are shown in Fig. 2.

Note that (5)–(6) is a periodic function of θ with period $2\pi k$. Furthermore,

$$\rho(2\pi l, k, \mu) = e^{i2\pi l/k}, \tag{7}$$

$$\rho(\pi + 2\pi l, k, \mu) = \frac{e^{i(2l+1)\pi/k}}{\sqrt[k]{1 + 2\mu}}. \tag{8}$$

The rotational and reflectional symmetries imply that

$$\rho(\theta + 2\pi l) = e^{i2\pi l/k}\rho(\theta), \tag{9}$$

$$\rho(\theta) = \overline{\rho(-\theta)} \tag{10}$$

and thus

$$\rho(\theta + l\pi) = e^{i2\pi l/k}\overline{\rho(l\pi - \theta)}.$$

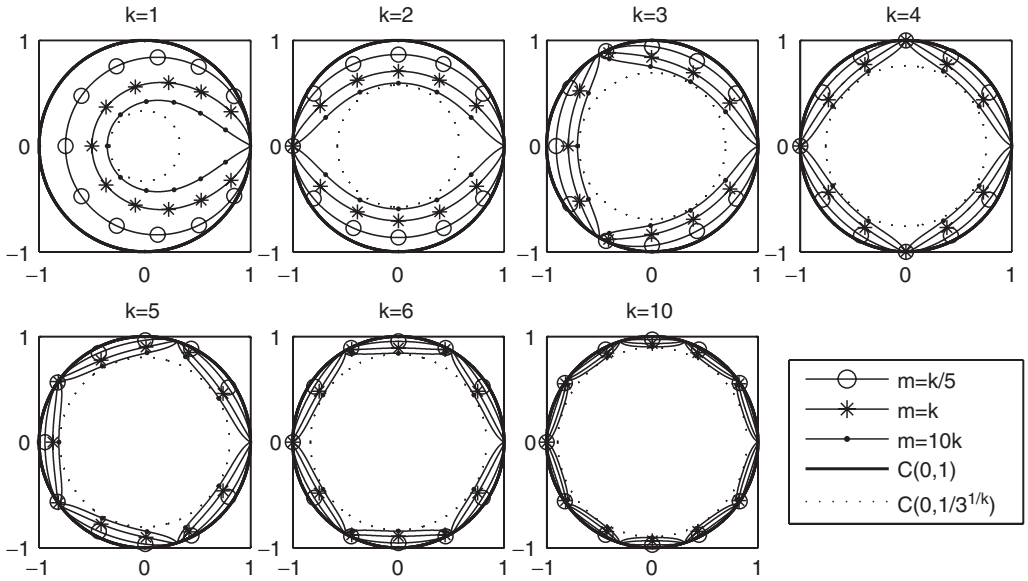

Fig. 2. Some of the Curves (4) for various values of k and m.

Property 2. *$|\rho|(\theta, k, \mu)$ is a decreasing function of θ and $\arg \rho(\theta, k, \mu)$ is an increasing function of θ on $[0, \pi]$. On $(0, \pi)$, $|\rho|(\theta, k, \mu)$ is a strictly decreasing function of θ and $\arg \rho(\theta, k, \mu)$ is a strictly increasing function of θ.*

Proof. This can be shown by analysing the derivatives of $|\rho|(\theta, k, \mu)$ and $\arg \rho(\theta, k, \mu)$, or equivalently, of $|\rho^k|(\theta, k, \mu)$ and $\arg \rho^k(\theta, k, \mu)$. Note also that $\rho^k(\theta, k, \mu) = \rho(\theta, 1, \mu)$. The computations can easily be done with a computer algebra system. □

Corollary 1. *Curve* (4) *is a closed curve and does not self-intersect.*

Proof. The first part follows from the continuity of ρ for $\theta \in [0, \pi]$, (7), (8) and the symmetry properties, or by noting that (5)–(6) is a continuous explicit parameterisation in θ with period $2\pi k$. The second part follows from Property 2 and the symmetry of the curve. □

Corollary 2. *$|\rho|$ has k maxima, reached at the vertices $e^{i2\pi l/k}$, $l = 0, \ldots, k-1$ of a regular k-gon. Hence the curve lies inside the unit circle. $|\rho|$ has k minima, reached at the points $(1/\sqrt[k]{1+2\mu})e^{i(2l+1)\pi/k}$, $l = 0, \ldots, k-1$, also vertices of a regular k-gon. Hence the open disc $D(0, 1/\sqrt[k]{1+2\mu})$ is contained within Curve* (4).

Proof. This follows immediately from (7), (8) and Property 2. □

Corollary 3. *The stability region $\Omega_1(k, m)$ is the area inside Curve* (4).

Proof. Note that $0 \in \Omega_1(k, m)$ since the roots of $P(\xi, 0, k, \mu, 1)$ are both zero. This point lies inside the curve. The point $\sqrt[k]{2} \notin \Omega_1(k, m)$, since the roots of $P(\xi, \sqrt[k]{2}, k, \mu, 1)$ are $1 + \mu \pm \sqrt{1+\mu^2}$. This point lies outside the curve. □

For all values of $\mu \in [0, 1)$, the open disk inside the circle with center point zero and radius $(\frac{1}{3})^{1/k}$ is contained within the stability region $\Omega_1(k, m)$. This is illustrated in Fig. 2 by the dotted circles. For any value of k, the line segment $[0, 1)$ is contained within $\Omega_1(k, m)$, and if k is even, the same holds for the line segment $(-1, 1)$.

Quite often, the map $\Phi_{\Delta t}$ has eigenvalues near 1 with small imaginary parts. Therefore, it is interesting to study the shape of $\Omega_1(k, m)$ near 1 in some more detail. In particular, we will look at $|\rho|$ as a function of $\arg \rho$.

For further study, we reparameterise the curve with parameter α, i.e.,

$$\rho(\alpha, k, \mu) = \rho(\theta(\alpha, k, \mu), k, \mu), \tag{11}$$

such that

$$\arg \rho(\alpha, k, \mu) = \arg \rho(\theta(\alpha, k, \mu), k, \mu) = \alpha.$$

Property 3. *Assume that* $0 \leqslant \mu < 1$, *and that k and* μ *are fixed. Near* $\rho = 1$ $(\alpha \approx 0)$,

$$|\rho|(\alpha, k, \mu) = 1 - \frac{1}{2}\frac{\mu(\mu+1)k}{(\mu-1)^2}(\alpha)^2 + \mathcal{O}(\alpha)^4.$$

Proof. We will first prove that $|\rho|(\alpha, k, \mu)$ is analytic at $\theta = 0$. Near $\theta = 0$, the explicit parameterisation (5) can be written as

$$\begin{cases} |\rho|(\theta, k, \mu) = \sqrt[2k]{\dfrac{1}{(1+\gamma_1) - \gamma_1 \cos(\theta)}}, \\ \arg \rho(\theta, k, \mu) = \dfrac{2\theta - \arctan(\gamma_1 \sin(\theta)/(\gamma_1 \cos(\theta) - 2\mu^2))}{k}, \end{cases}$$

where $\gamma_1 = 2\mu(1+\mu)$.

Both expressions are analytic at $\theta = 0$. Now

$$\frac{\partial |\rho|(\alpha, k, \mu)}{\partial \alpha} = \frac{\partial |\rho|(\theta, k, \mu)}{\partial \theta}\,\frac{\partial \theta(\alpha, k, \mu)}{\partial \alpha}.$$

Since $\theta(\alpha, k, \mu)$ is defined by $\arg \rho(\theta(\alpha, k, \mu), k, \mu) = \alpha$, we have

$$\frac{\partial \arg \rho(\theta, k, \mu)}{\partial \theta}\,\frac{\partial \theta(\alpha, k, \mu)}{\partial \alpha} = 1,$$

and thus

$$\frac{\partial |\rho|(\alpha, k, \mu)}{\partial \alpha} = \frac{\partial |\rho|(\theta, k, \mu)/\partial \theta}{\partial \arg \rho(\theta, k, \mu)/\partial \theta}. \tag{12}$$

Similarly,

$$\frac{\partial^n |\rho|(\alpha, k, \mu)}{\partial \alpha^n} = \frac{\partial/\partial\theta(\partial^{n-1}|\rho|(\alpha, k, \mu)/\partial \alpha^{n-1})}{\partial \arg \rho(\theta, k, \mu)/\partial \theta}. \tag{13}$$

Since $\partial \arg \rho(\theta, k, \mu)/\partial\theta = (1-\mu)/k$ at $\theta = 0$, $|\rho|(\alpha, k, \mu)$ is also analytic at $\theta = 0$ for $0 \leqslant \mu < 1$.

Because of the reflectional symmetry, $|\rho|(\alpha, k, \mu)$ is an even function of α and all odd-order derivatives must be 0. Using (12) and (13), it is then straightforward to compute the Taylor series of $|\rho|(\alpha, k, \mu)$ in α. □

For $\mu = 1$, the tangent vector at $\theta = 0$ cannot be determined from the representation in polar coordinates since both $\partial|\rho|(\theta, k, \mu)/\partial\theta$ and $\partial(\arg \rho(\theta, k, \mu))/\partial\theta$ are zero. However, one can verify that after transformation to Cartesian coordinates $x = \mathrm{Re}(\rho(\theta, k, \mu))$ and $y = \mathrm{Im}(\rho(\theta, k, \mu))$,

$$\lim_{\theta \to 0+} \frac{\mathrm{d}x/\mathrm{d}\theta}{\sqrt{(\mathrm{d}x/\mathrm{d}\theta)^2 + (\mathrm{d}y/\mathrm{d}\theta)^2}} = -1, \quad \lim_{\theta \to 0-} \frac{\mathrm{d}x/\mathrm{d}\theta}{\sqrt{(\mathrm{d}x/\mathrm{d}\theta)^2 + (\mathrm{d}y/\mathrm{d}\theta)^2}} = +1$$

and

$$\lim_{\theta \to 0} \frac{\mathrm{d}y/\mathrm{d}\theta}{\sqrt{(\mathrm{d}x/\mathrm{d}\theta)^2 + (\mathrm{d}y/\mathrm{d}\theta)^2}} = 0,$$

and the curve has a cusp-shaped singularity at 1.

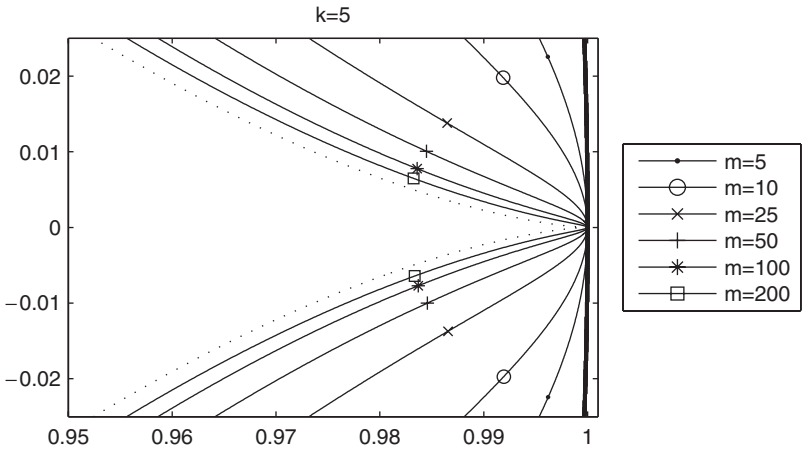

Fig. 3. Tip formation as μ increases. The thick line represents the unit circle. The thin lines are stability region boundaries for a fixed value of k (5) and various values of m (5, 10, 25, 50, 100 and 200). The dotted line is the limiting stability region boundary for $\mu = 1$.

The shape of the tip for $k = 5$ and various values of μ is shown in Fig. 3. Note that as μ increases towards 1, the tip becomes more narrow and approaches the singular limit case for $\mu = 1$. The stability region of the PIM with linear extrapolation does not exhibit such a tip formation, but splits into two disjunct regions when $\mu \approx 0.72$.

Fig. 3 also suggests that the stability regions shrink as m is increased, while k is kept constant.

Property 4. *Let* $\mu_1, \mu_2 \in [0, 1]$. *Then* $\Omega_1(k, \mu_1) \subset \Omega_1(k, \mu_2) \Leftrightarrow \mu_1 > \mu_2$.

Proof. We first look at how $|\rho|(\alpha, k, \mu)$ changes as μ is increased. For $\alpha = 0$, $|\rho| = 1$ irrespective of the value of μ. For $\arg \rho = \pi/k$,

$$|\rho| = \sqrt[k]{\frac{1}{1+2\mu}}.$$

It is easily verified that this is a strictly decreasing function of μ for $0 \leqslant \mu \leqslant 1$. For $\arg \rho \in (0, \pi/k)$, we consider again the parameterisation (11). Now

$$\frac{\partial |\rho|(\alpha, k, \mu)}{\partial \mu} = \frac{\partial |\rho|(\theta, k, \mu)}{\partial \theta} \frac{\partial \theta(\alpha, k, \mu)}{\partial \mu} + \frac{\partial |\rho|(\theta, k, \mu)}{\partial \mu}.$$

Since $\theta(\alpha, k, \mu)$ is defined by $\arg \rho(\theta, k, \mu) = \alpha$, we have

$$\frac{\partial \arg \rho(\theta, k, \mu)}{\partial \theta} \frac{\partial \theta}{\partial \mu} + \frac{\partial \arg \rho(\theta, k, \mu)}{\partial \mu} = 0,$$

and hence

$$\frac{\partial |\rho|(\alpha, k, \mu)}{\partial \mu} = -\frac{\partial |\rho|(\theta, k, \mu)}{\partial \theta} \frac{\partial \arg \rho(\theta, k, \mu)/\partial \mu}{\partial \arg \rho(\theta, k, \mu)/\partial \theta} + \frac{\partial |\rho|(\theta, k, \mu)}{\partial \mu}. \tag{14}$$

For $\theta \in (0, \pi/k)$, the explicit parameterisation (5) can be written as

$$\begin{cases} |\rho|(\theta, k, \mu) = \sqrt[2k]{\dfrac{1}{(1+\gamma_1) - \gamma_1 \cos(\theta)}}, \\ \arg \rho(\theta, k, \mu) = \dfrac{2\theta - \operatorname{arccot}\left(\frac{\gamma_1 \cos(\theta) - 2\mu^2}{\gamma_1 \sin(\theta)}\right)}{k}, \end{cases} \tag{15}$$

where $\gamma_1 = 2\mu(1+\mu)$. Substituting (15) in (14), it can be shown (with the help of a computer algebra system) that (14) is negative for all values of $\alpha \in (0, \pi/k)$ (corresponding to $\theta \in (0, \pi)$) and for all $k \in \mathbb{N}_0$. This proofs the property. □

Since the stability region of the method is not the whole unit circle and shrinks as μ is increased, the extrapolation step size will often be limited even if the spectrum of the inner integrator is contained within the unit circle.

3.2. Stability analysis of the scheme with quadratic extrapolation

In this case, the stability polynomial (2) reduces to

$$P(\xi, \rho, k, \mu, 2) \equiv \xi^3 - \frac{(\mu+1)(\mu+2)}{2}\rho^k\xi^2 + \mu(\mu+2)\rho^k\xi - \frac{\mu(\mu+1)}{2}\rho^k. \tag{16}$$

The boundary of the stability domain lies on the curve

$$P(\mathrm{e}^{\mathrm{i}\theta}, \rho(\theta), k, \mu, 2) = 0, \tag{17}$$

and an explicit parameterisation for this curve is

$$\rho(\theta, k, \mu) = \sqrt[k]{\frac{\mathrm{e}^{\mathrm{i}3\theta}}{((\mu+1)(\mu+2)/2)\mathrm{e}^{\mathrm{i}2\theta} - \mu(\mu+2)\,\mathrm{e}^{\mathrm{i}\theta} + \mu(\mu+1)/2}} = \sqrt[k]{\rho(\theta, 1, \mu)}, \tag{18}$$

where we take the root such that

$$\arg\rho \in \left((2l-1)\frac{\pi}{k}, (2l+1)\frac{\pi}{k}\right] \quad \text{if } \theta \in ((2l-1)\pi, (2l+1)\pi]. \tag{19}$$

The rotational and reflectional symmetries again imply Eqs. (9) and (10).

Fig. 4 shows the curves for various values of k and μ. Note that $\rho(\theta, k, \mu)$ is a periodic function of θ with period $2\pi k$. Furthermore,

$$\rho(2\pi l, k, \mu) = \mathrm{e}^{\mathrm{i}2\pi l/k} \tag{20}$$

$$\rho(\pi + 2\pi l, k, \mu) = \frac{\mathrm{e}^{\mathrm{i}(2l+1)\pi/k}}{\sqrt[k]{2\mu^2 + 4\mu + 1}}. \tag{21}$$

Unlike in the previous section, it is more difficult to prove that the parameterisation (18)–(19) is continuous in its parameter θ. It is necessary to show that $\rho(\theta, 1, \mu)$ does not intersect with the negative real axis if $\theta \in (-\pi, \pi)$ for if $\rho(\theta, 1, \mu)$ would intersect, (19) would result in a jump $\pm 2\pi$ of $\arg\rho(\theta, 1, \mu)$ at every intersection, and a corresponding jump of $\pm 2\pi/k$ of $\arg\rho(\theta, k, \mu)$.

Property 5. *The arc $\rho(\theta, 1, \mu)$ with $\theta \in (0, \pi)$ does not intersect the negative real axis. It has two intersections with the positive real axis if $\gamma < \mu \leqslant 1$, with $\gamma = -\frac{2}{3} + \frac{1}{3}\sqrt[3]{19 - 3\sqrt{33}} + \frac{1}{3}\sqrt[3]{19 + 3\sqrt{33}} \approx 0.839287\ldots$, and no intersections if $0 \leqslant \mu < \gamma$. If $\mu = \gamma$, the arc $\rho(\theta, 1, \mu)$ is tangent to the positive real axis.*

Proof. Since the denominator of $\rho(\theta, 1, \mu)$ cannot be 0, $\rho(\theta, 1, \mu)$ is clearly a continuous function of θ. To study the intersections of the arc $\rho(\theta, 1, \mu)$, $\theta \in (0, \pi)$ with the real axis, one can multiply the numerator and denominator of $\rho(\theta, 1, \mu)$ with the complex conjugate of the denominator to make the denominator real, and then look for all zeroes of the imaginary part of the numerator. This is a lengthy calculation, but the above result can be obtained with the help of a computer algebra system. The same value of γ was derived in [9] using the Routh–Hurwitz criterion. □

Now $\rho(\theta, 1, \mu)$ is a continuous function of θ on $[-\pi, \pi]$. Moreover, for a small enough value of ε, $\mathrm{Im}(\rho(\theta, 1, \mu)) > 0$ for $\theta \in (\pi - \varepsilon, \pi)$ and $\mathrm{Im}(\rho(\theta, 1, \mu)) < 0$ for $\theta \in (-\pi, -\pi + \varepsilon)$. Together with Property 5, this implies that (18)–(19) is a continuous function of θ.

Property 5 also implies that, unlike in the linear extrapolation case, $\arg\rho(\theta, k, \mu)$ will not be strictly decreasing in θ for all values of k and μ.

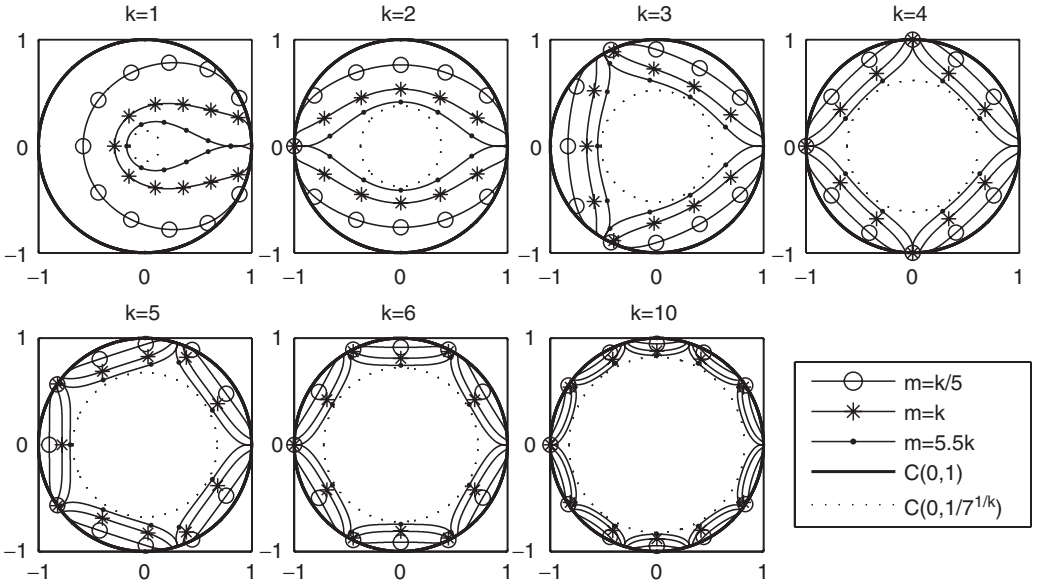

Fig. 4. Some of the Curves (17) for various values of k and m.

Property 6. *$|\rho|(\theta, k, \mu)$ is a decreasing function of θ on $[0, \pi]$. On $(0, \pi)$, $|\rho|(\theta, k, \mu)$ is a strictly decreasing function of θ.*

Proof. This can be shown by analysing the derivative of $|\rho|(\theta, k, \mu)$ using a computer algebra system. □

Corollary 4. *Curve* (17) *is a closed curve which does not self-intersect if $\mu < \gamma$, while it does self-intersect if $\mu > \gamma$. In the latter case, there are exactly $2k$ intersection points, namely 2 points along each half line $L_j = \{\rho | \arg \rho = 2\pi j/k, |\rho| \geqslant 0\}$ with $j = 0, 1, \ldots, k-1$.*

Proof. Curve (17) is closed since it can be described by (18)–(19), an explicit and continuous parameterisation with period $2\pi k$. The second part of the corollary follows by combining Properties 5 and 6 with the symmetry properties. □

Corollary 5. *$|\rho|$ has k maxima, reached at the vertices $e^{i2\pi l/k}$, $l = 0, \ldots, k-1$ of a regular k-gon, i.e., the curve lies inside the unit circle. $|\rho|$ has k minima, reached at the points $(1/\sqrt[k]{2\mu^2 + 4\mu + 1})\, e^{i(2l+1)\pi/k}$, $l = 0, \ldots, k-1$, also vertices of a regular k-gon. Hence the open disc $D(0, 1/\sqrt[k]{2\mu^2 + 4\mu + 1})$ is contained within Curve* (17).

Proof. This follows immediately from (20), (21) and Property 6. □

Corollary 6. *If $\mu \leqslant \gamma$, the stability region $\Omega_2(k, m)$ is the area inside Curve* (17). *If $\mu > \gamma$, the stability region $\Omega_2(k, m)$ consists of $k+1$ disjunct regions: the large region containing* 0, *and k smaller regions near $e^{i\pi l/k}$ $(l = 0, \ldots, k-1)$.*

Proof. Due to the symmetry properties and Corollary 4, it suffices to study the intersection of the stability region with the interval $[0, 1)$. The coefficients of the stability polynomial (16) will then be real. After the substitution $\xi = (1+\chi)/(1-\chi)$ (to transform the unit disk to the left half plane), we can apply the Routh–Hurwitz criterion to determine the real stability interval. If $\mu < \gamma$, this interval is $[0, 1)$. If $\mu \geqslant \gamma$, this interval is $[0, x_1) \cup (x_2, 1)$ with x_1 and x_2 the two intersection points of (17) with the real positive axis on $(0, 1)$. □

For all values of $\mu \in [0, 1)$, the open disk inside the circle with center point zero and radius $(\frac{1}{7})^{1/k}$ is contained within the stability region $\Omega_2(k, m)$. This is illustrated in Fig. 4 by the dotted circles.

Again, it is interesting to look at the shape of the stability region near 1.

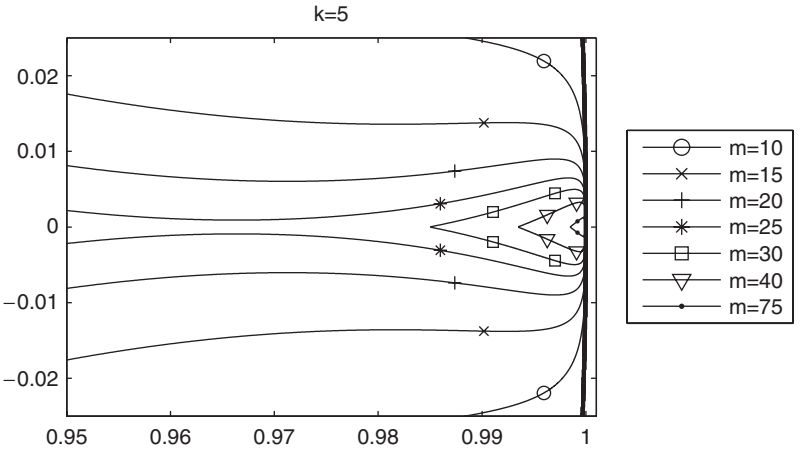

Fig. 5. Detailed view of the stability regions $\Omega_2(5, m)$ near 1 for various values of m. The thick line represents the unit circle. The thin lines are stability region boundaries for a fixed value of $k = 5$ and various values of m (10, 15, 20, 25, 30, 40, 75). No tip is formed but the stability region falls apart and the regions near 1 shrink fast for increasing values of m.

Property 7. *Assume that* $0 \leqslant \mu < 1$, *and that k and* μ *are fixed. Near* $\rho = 1$ $(\alpha \approx 0)$,

$$|\rho|(\alpha, k, \mu) = 1 - \frac{\mu(\mu+1)^2(\mu+2)k^3}{8(\mu-1)^4}(\alpha)^4 + \mathcal{O}(\alpha)^6. \tag{22}$$

Proof. As in the linear extrapolation case, we will first show that $|\rho|(\alpha, k, \mu)$ is analytic at $\theta = 0$. Near $\theta = 0$, the explicit parameterisation (18) can be written as

$$\begin{cases} |\rho|(\theta, k, \mu) = \sqrt[2k]{\dfrac{1}{(1+\gamma_2) - 2\gamma_2\cos(\theta) + \gamma_2\cos(\theta)^2}}, \\ \arg\rho(\theta, k, \mu) = \dfrac{3\theta - \arctan\left(\frac{(\gamma_2/\mu)\sin(2\theta) - 2(\gamma_2/(\mu+1))\sin(\theta)}{(\gamma_2/\mu)\cos(2\theta) - 2(\gamma_2/(\mu+1))\cos(\theta) + (\gamma_2/(\mu+2))}\right)}{k}, \end{cases}$$

where $\gamma_2 = \mu(\mu+1)^2(\mu+2)$.

Both expressions are analytic at $\theta = 0$. Using Eqs. (12) and (13), and the fact that $\partial \arg\rho(\theta, k, \mu)/\partial\theta = (1-\mu)/k$ at $\theta = 0$, this implies that $|\rho|(\alpha, k, \mu)$ is also analytic at $\theta = 0$ for $0 \leqslant \mu < 1$.

Because of the reflectional symmetry, $|\rho|(\alpha, k, \mu)$ is an even function of α and all odd-order derivatives must be 0. Using (12) and (13), it is then straightforward to compute the Taylor series of $|\rho|(\alpha, k, \mu)$ in α. □

Note that (22) has no second order term in α. For $\mu = 1$, the tangent vector at $\theta = 0$ can again not be determined from the representation in polar coordinates since both $\partial|\rho|(\theta, k, \mu)/\partial\theta$ and $\partial(\arg\rho(\theta, k, \mu))/\partial\theta$ are zero. However, one can verify that after transformation to Cartesian coordinates $x = \mathrm{Re}(\rho(\theta, k, \mu))$ and $y = \mathrm{Im}(\rho(\theta, k, \mu))$,

$$\lim_{\theta\to 0} \frac{\mathrm{d}x/\mathrm{d}\theta}{\sqrt{(\mathrm{d}x/\mathrm{d}\theta)^2 + (\mathrm{d}y/\mathrm{d}\theta)^2}} = 0 \quad \text{and} \quad \lim_{\theta\to 0} \frac{\mathrm{d}y/\mathrm{d}\theta}{\sqrt{(\mathrm{d}x/\mathrm{d}\theta)^2 + (\mathrm{d}y/\mathrm{d}\theta)^2}} = -1,$$

and the curve will thus be tangent to the unit circle at 1.

The shape of the stability regions $\Omega_2(k, m)$ near 1 for $k = 5$ and various values of μ are shown in Fig. 5. We see that contrary to the schemes with linear extrapolation, no cusp is formed, and that the stability regions approximate the unit circle very well near 1. However, the usage of the method with quadratic extrapolation will often be limited for values of $\mu > \gamma$, especially because the k small stability regions near $\mathrm{e}^{\mathrm{i}\pi l/k}(l = 0, \ldots, k-1)$ shrink fast when μ grows.

Property 8. *Suppose that $\mu > \gamma$. If μ grows towards 1, then the intersection of the stability domain $\Omega_2(k, m)$ and the positive real axis is approximately*

$$\left[0, \sqrt[k]{\frac{1}{2}}\left(1 - \frac{2(\mu-1)}{k} + \mathcal{O}((\mu-1)^2)\right)\right) \cup \left(1 - \frac{3}{2k}(\mu-1)^2 + \mathcal{O}((\mu-1)^3), 1\right).$$

Proof. In the proof of Property 5 we mentioned that it is possible to obtain an analytical expression for the intersection points of curve (18) with the real axis. The result above is then obtained by computing the Taylor series expansions of these expressions about $\mu = 1$. □

Note that the stability regions of the PIM with quadratic extrapolation split into two disjunct regions when $\mu \approx 0.7$. However, the diameter of the part at 1 shrinks linearly if $\mu \to 1$.

Property 9. *Let $\mu_1, \mu_2 \in [0, 1]$. Then $\Omega_2(k, \mu_1) \subset \Omega_2(k, \mu_2) \Leftrightarrow \mu_1 > \mu_2$.*

Proof. Again, we shall restrict ourselves to the study of the stability region in the sector R. For $\arg\rho = 0$, $|\rho| = 1$ irrespective of the value of μ. For $\arg\rho = \pi/k$,

$$|\rho| = \sqrt[k]{\frac{1}{2\mu^2 + 4\mu + 1}}.$$

It is easily verified that this is a strictly decreasing function of μ for $0 \leqslant \mu \leqslant 1$.

For $\arg\rho \in (0, \pi/k)$, we cannot reuse Eq. (14), since $\partial \arg\rho(\theta, k, \mu)/\partial\theta$ is 0 for certain values of $k \in \mathbb{N}_0$, $\mu \in [0, 1)$ and $\theta \in (0, \pi)$. Therefore, we reparameterise $\rho(\theta, k, \mu)$ with parameter β, i.e., $\rho(\beta, k, \mu) = \rho(\theta(\beta, k, \mu), k, \mu)$ such that $\mathrm{Re}(\rho(\beta, k, \mu)) = \mathrm{Re}(\rho(\theta(\beta, k, \mu), k, \mu)) = \beta$. We can then derive, in an analogue way as in the proof of Property 4, that

$$\frac{\partial \,\mathrm{Im}(\rho(\beta, k, \mu))}{\partial\mu} = -\frac{\partial \,\mathrm{Im}(\rho(\theta, k, \mu))}{\partial\theta}\frac{\partial \,\mathrm{Re}(\rho(\theta, k, \mu))/\partial\mu}{\partial \,\mathrm{Re}(\rho(\theta, k, \mu))/\partial\theta} + \frac{\partial \,\mathrm{Im}(\rho(\theta, k, \mu))}{\partial\mu}. \tag{23}$$

It can be shown (with the help of a computer algebra system) that $\partial \,\mathrm{Re}(\rho(\theta, k, \mu))/\partial\theta \neq 0$ for $\theta \in (0, \pi)$, and that (23) is negative for all values of $\theta \in (0, \pi)$. This proves the property. □

3.3. Stability regions for acceleration schemes based on higher order extrapolation

In this section, we will not give a detailed stability analysis of Algorithm 1 with $N > 2$, but we briefly show that there are important differences compared to the case where $N = 1$ or $N = 2$, which make methods based on higher order extrapolations less attractive.

As explained in the previous sections, the curve $\rho(\theta)$, implicitly defined by $P(e^{i\theta}, \rho(\theta), k, \mu, N) = 0$ plays a crucial role when determining the stability region boundary of the method. Since $\sum_{j=0}^{N} l_j = 1$, it is clear from Eq. (2) that 1 will always lie on this curve. Furthermore, it can be shown that this curve will always be tangent to the unit circle at 1 if $0 \leqslant \mu < 1$ for all $N \in \mathbb{N}_0$. For $N = 1$ and $N = 2$, we also showed that this curve is contained within the unit circle. For higher values of N, it turns out that this is no longer true. For $N = 3$ for instance, this can be seen from the Taylor series expansion of $|\rho|(\alpha, k, \mu)$ about $\alpha = 0$,

$$|\rho|(\alpha, k, \mu) = 1 + \frac{\mu(\mu+1)(\mu+2)(\mu+3)k^3}{24(\mu-1)^4}(\alpha)^4 + \mathcal{O}(\alpha)^6,$$

which has a positive coefficient in the second term of the Taylor series. This means that an unstable time-stepper may be stabilised by the acceleration scheme. This property is illustrated in Fig.6. For large values of μ, the stability region splits, just like in the case with $N = 2$. Applying the Routh–Hurwitz conditions reveals that this split happens when $\mu \approx 0.63$, which corresponds to a speedup of 2.7. Fig. 6 also shows in detail that if μ is further increased, the small parts of the stability region at the points $e^{i\pi l/k}$ $(l = 0, \ldots, k-1)$ shrink until they disappear at $\mu \approx 0.73$. This means that the slow modes near 1 cannot be integrated in a stable manner anymore (we are losing zero-stability), which makes the method useless for most purposes. Both critical values of μ were also reported in [9].

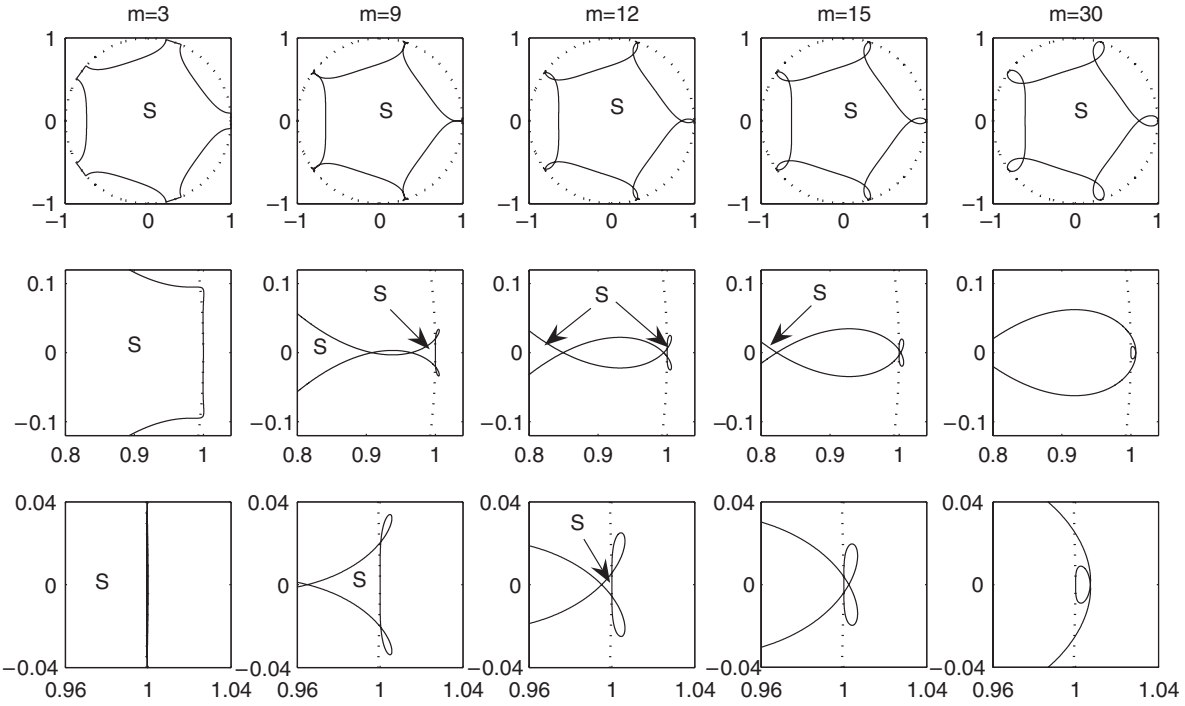

Fig. 6. The curve $P(e^{i\theta}, \rho(\theta), 5, \mu, 3) = 0$ for several values of μ. In each column, subsequent close-ups of the same curve are shown. The parts corresponding to the stability region (that are still visible) are indicated by the letter S. The dotted line is the unit circle.

For higher values of N, similar problems arise at even smaller values of μ. For this reason, we shall restrict our numerical experiments to values of N up to 3.

4. Numerical illustration

In this section we will study the performance and properties of Algorithm 1 for a linear convection–diffusion PDE time-stepper code. Though acceleration of explicit methods for PDEs is not the target application for our scheme, this problem is a good example to illustrate some of the stability properties from the previous section. The numerical experiments will also give an idea about the accuracy of the method.

4.1. A convection–diffusion PDE time-stepper code

We briefly describe the time-stepper code used in our experiments. The one-dimensional linear convection–diffusion PDE

$$\frac{\partial u}{\partial t} = a\frac{\partial^2 u}{\partial x^2} + b\frac{\partial u}{\partial x} \tag{24}$$

with periodic boundary conditions has been spatially discretised on [0, 1] using second order central differences for the diffusion term and first order upwind differences for the convection term. The values of a and b are chosen to be 0.01 and 2. A spatial grid spacing of $\Delta x = 10^{-3}$ is used in order to get an acceptable discretisation error. For our time-stepper (1), we use the forward Euler method with step size $\Delta t = 4 \times 10^{-5}$, determined by stability constraints. In our experiments, we use a scaled and shifted box function as initial condition (see Fig. 7 (left)). The left part of Fig. 7 shows some snapshots of the solution at several moments in time ($t = 0, 0.1, 0.2, \ldots, 0.5$). The eigenvalue spectrum of the time-stepper is shown in the right part of Fig. 7. It is clear that the time step Δt was chosen close to the stability boundary for the forward Euler scheme. For the problem at hand we can numerically verify—using a much

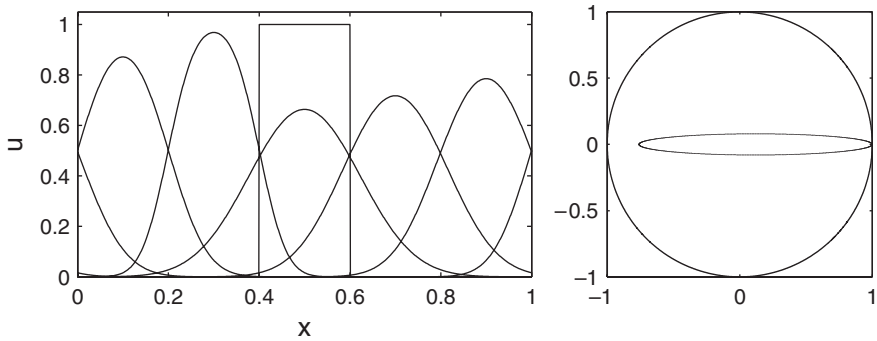

Fig. 7. Some snapshots of the time-dependent reference solution $u^*(t)$ of the convection–diffusion problem at $t = 0, 0.1, 0.2, \ldots, 0.5$. The initial condition is the scaled and shifted box function in the middle of the interval. The eigenvalues of the time-stepper are shown on the right.

Table 1
$-\log_{10}(e)$, the number of correct digits of the solution, for $N = 1$

$k\backslash m$	1	2	3	4	5	6	7	8	9	10	k	$2k$	$3k$
1	⋆	⋆	⋆	⋆	⋆	⋆	⋆	⋆	⋆	⋆	⋆	⋆	⋆
2	2.5	2.0	1.7	1.4	1.2	1.1	0.9	0.8	0.6	0.5	2.0	1.4	1.1
3	2.5	2.1	1.8	1.6	1.4	1.2	⋆	⋆	⋆	⋆	1.8	1.2	⋆
4	2.6	2.1	1.9	1.7	1.5	1.3	1.2	1.1	1.0	0.9	1.7	1.1	0.7
5	2.6	2.2	1.9	1.7	1.6	1.4	1.3	1.2	1.1	1.0	1.6	1.0	0.5
6	2.6	2.2	2.0	1.8	1.6	1.5	1.4	1.2	1.1	1.0	1.5	0.9	0.5
7	2.6	2.3	2.0	1.8	1.7	1.5	1.4	1.3	1.2	1.1	1.4	0.8	0.2
8	2.7	2.3	2.0	1.8	1.7	1.6	1.4	1.3	1.2	1.2	1.3	0.7	⋆
9	2.7	2.3	2.1	1.9	1.7	1.6	1.5	1.4	1.3	1.2	1.3	0.6	⋆
10	2.7	2.3	2.1	1.9	1.7	1.6	1.5	1.4	1.3	1.2	1.2	0.6	⋆

finer spatial and temporal mesh—that the spatial discretisation error, measured in the infinity norm, is about 0.02 at $t = 0.5$. We will compare errors introduced by Algorithm 1 with this discretisation error.

4.2. Acceleration of the convection–diffusion time-stepper with Algorithm 1

We now compare the trajectory computed by the convection–diffusion time-stepper with the trajectory computed by the accelerated time-stepper. We define the error e of the accelerated scheme at time $t = 0.5$ as

$$e = \|u^*(0.5) - \overline{u}(0.5)\|_\infty,$$

where $u^*(0.5)$ represents the solution computed with the time-stepper at $t = 0.5$ (after 12 500 time steps), and $\overline{u}(0.5)$ represents the solution computed with Algorithm 1. Since the accelerated scheme does not necessarily compute a solution at $t = 0.5$, an interpolation method is used to determine $\overline{u}(0.5)$.

In Tables 1–3, we show $-\log_{10}(e)$ (the number of digits of $\overline{u}(0.5)$ corresponding to those of $u^*(0.5)$) for various values of k, m and N. If none of the computed digits is correct, we have put a ⋆. If the acceleration method is unstable, i.e., if not all eigenvalues ρ of the original time-stepper lie within the stability region of the acceleration method, the entries in the table are underlined. Several things are noteworthy. As we can expect, for a fixed value of k, the accuracy decreases as m is increased. Each method ultimately becomes unstable for large values of m (cf. Properties 4 and 9). For a fixed value of m, the accuracy increases as k is increased. We also see that choosing $k = 1$ is not very useful here, since only very small extrapolation steps can be taken due to the method's poor stability properties. Using $k > 1$ (one of our extensions to [9]) can thus be useful for applications with complex eigenvalues. For a constant speedup (and thus a constant ratio m/k), the method becomes less accurate as k and m increase. The results for k even are better due

Table 2
$-\log_{10}(e)$, the number of correct digits of the solution, for $N = 2$

$k\backslash m$	1	2	3	4	5	6	7	8	9	10	k	$2k$	$3k$
1	⋆	⋆	⋆	⋆	⋆	⋆	⋆	⋆	⋆	⋆	⋆	⋆	⋆
2	5.1	4.5	4.1	3.8	3.5	3.3	⋆	⋆	⋆	⋆	4.5	3.8	3.3
3	5.1	⋆	⋆	⋆	⋆	⋆	⋆	⋆	⋆	⋆	⋆	⋆	⋆
4	5.1	4.5	4.2	3.9	3.7	3.5	3.3	3.2	3.0	2.9	3.9	3.2	⋆
5	5.0	4.5	4.2	3.9	3.7	3.5	3.4	⋆	⋆	⋆	3.7	⋆	⋆
6	5.0	4.5	4.2	3.9	3.7	3.5	3.4	3.3	3.1	3.0	3.5	2.8	⋆
7	4.9	4.5	4.2	3.9	3.7	3.6	3.4	3.3	3.2	3.0	3.4	2.7	⋆
8	4.9	4.5	4.2	3.9	3.7	3.6	3.4	3.3	3.2	3.1	3.3	2.6	⋆
9	4.9	4.4	4.1	3.9	3.7	3.6	3.4	3.3	3.2	3.1	3.2	2.5	⋆
10	4.8	4.4	4.1	3.9	3.7	3.6	3.4	3.3	3.2	3.1	3.1	1.7	⋆

Table 3
$-\log_{10}(e)$, the number of correct digits of the solution, for $N = 3$

$k\backslash m$	1	2	3	4	5	6	7	8	9	10	k	$2k$	$3k$
1	⋆	⋆	⋆	⋆	⋆	⋆	⋆	⋆	⋆	⋆	⋆	⋆	⋆
2	7.6	6.8	⋆	⋆	⋆	⋆	⋆	⋆	⋆	⋆	6.8	⋆	⋆
3	⋆	⋆	⋆	⋆	⋆	⋆	⋆	⋆	⋆	⋆	⋆	⋆	⋆
4	7.3	6.7	6.3	5.9	5.6	⋆	⋆	⋆	⋆	⋆	5.9	⋆	⋆
5	7.2	6.6	⋆	⋆	⋆	⋆	⋆	⋆	⋆	⋆	⋆	⋆	⋆
6	7.1	6.6	6.2	5.9	5.6	5.4	5.2	⋆	⋆	⋆	5.4	⋆	⋆
7	7.0	6.5	6.1	5.8	5.6	5.4	5.2	5.0	⋆	⋆	5.2	⋆	⋆
8	6.9	6.4	6.1	5.8	5.6	5.4	5.2	5.0	4.0	⋆	5.0	⋆	⋆
9	6.8	6.4	6.0	5.8	5.5	5.3	5.2	5.0	4.9	2.6	4.9	⋆	⋆
10	6.8	6.3	6.0	5.7	5.5	5.3	5.1	5.0	4.9	4.7	4.7	⋆	⋆

to the symmetry properties of the stability regions. Higher order extrapolations lead to methods that are more accurate for the same values of k and m, but turn out to be less stable (cf. Section 3.3).

It is also clear that for this problem, acceleration methods based on a linear extrapolation are not very useful, since e is large compared to the discretisation error. The methods based on a third order extrapolation yield very accurate results, but suffer from severe stability restrictions. Moreover, the high accuracy of these methods is of no benefit in this example, since the overall error will still be determined by the discretisation error. The methods based on a quadratic extrapolation are clearly a good compromise between stability and accuracy, and admit a speedup $S = 3.5$ without substantial loss of the overall accuracy.

Fig. 8 shows the eigenvalue spectrum of the convection–diffusion time-stepper, together with the stability regions $\Omega_2(2, 8)$ and $\Omega_2(5, 7)$. This figure illustrates that stability might be lost due to the complex eigenvalues near 1, or due to the eigenvalues with smallest real part. It is clear that the complex eigenvalues near 1—due to convective character of Eq. (7)—are most restrictive, since k can always be chosen such that the stability region encloses the eigenvalues with smallest real part for any value of m (cf. Corollaries 2 and 5). Indeed, if we set $b = 0$ and use Algorithm 1 with $N = 1$ and $k = 2$, the attainable speedup will solely be determined by the required accuracy (cf. Corollaries 1 and 2). Specifically, if we are satisfied with an error of the size of the discretisation error ($e \approx 0.02$), we are able to achieve a speedup $S = 23$.

4.3. Comparison with projective integration

In this section, we compare our scheme to the PIMs of [2,3]. These are the only other schemes known to us designed to accelerate (1) without relying on the precise definition of the map.

The stability regions of the PIM with linear extrapolation are only connected if $S < 4.6$ (see [2]). As $m \to \infty$, the stability region approaches two disks, one centered at the origin with radius $(1/m)^{1/(k-1)}$, and another centered at

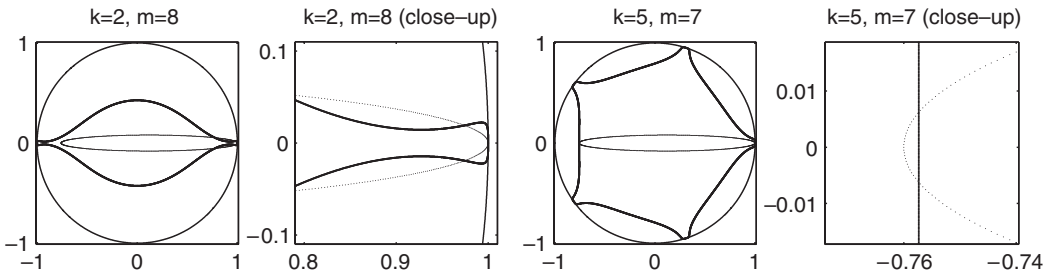

Fig. 8. The eigenvalue spectrum of the convection–diffusion time-stepper and the boundaries of the stability regions $\Omega_2(2, 8)$ and $\Omega_2(5, 7)$. Stability might get lost due to the imaginary eigenvalues near 1, or due to the real eigenvalues with smallest real part.

Table 4
The minimal value of k and the number of correct digits $E := -\log_{10}(e)$ for the PIM and SPIM, for several values of N and S

N	S	PIM		SPIM	
		$k_{\min}$	E	$k_{\min}$	E
1	2	13	1.9	3	2.4
1	3	16	1.4	4	1.9
1	4	19	1.0	8	1.4
2	2	28	3.6	6	4.7
2	3	34	2.8	30	2.3
2	4	⋆	⋆	⋆	⋆
3	2	48	4.9	10	6.3
3	3	⋆	⋆	⋆	⋆
3	4	⋆	⋆	⋆	⋆

$1 - 1/m$ with radius $1/m$. Similar results can be obtained for schemes based on higher order extrapolation methods. For the acceleration of a time-stepper with a band of eigenvalues as in our test case, this implies that only values of S up to about 4 are feasible. Moreover, for our model problem, the value of k must be quite large in order to capture the leftmost eigenvalues of the time-stepper in the stability region, even for a small speedup S. This means that if we are interested in a method with a given speedup, the value of m will also have to be quite large, which has consequences for the accuracy of the method. Table 4 shows the minimal value of k and the corresponding error for the PIM with $N = 1, 2$ and 3, and for several values of S. Similar to the numerical results of Algorithm 1, the most accurate stable schemes to obtain a speedup $S = 2, 3$ and 4 are those using cubic, quadratic and linear extrapolation, respectively. For our model problem, Algorithm 1 yields more accurate results than the PIM for all values of S.

Rather than extrapolating through the last two points, one can also use the last and third last point. For such a scheme the stability region becomes symmetric about the imaginary axis and extends further in the negative half plane. We will denote this method by SPIM, referring to the symmetry of the stability regions. This adaptation has almost no influence on the range of attainable speedup values for which the stability regions are connected. The minimal value of k and the corresponding error for the SPIM with $N = 1, 2$ and 3, and for several values of S are also shown in Table 4. Again, the most accurate schemes to obtain a speedup $S = 2, 3$ and 4 are those using cubic, quadratic and linear extrapolation, respectively. For our model problem, the modification of the PIM results in a more efficient scheme. However, for $S = 2$ and $S = 3$, and using the best value of N, the results of Algorithm 1 are still more accurate than the results obtained with SPIM. Only for $S = 4$ the SPIM yields a more accurate result. In that case however the error is larger than the discretisation error, which makes neither of both methods really useful.

Finally, Table 5 shows for each method the optimal value of S and the corresponding value of N for a given accuracy. We note that the degree of the extrapolating polynomial increases if the desired accuracy is increased. Furthermore, our method is at least as efficient as (and in some cases even better than) the PIM or the SPIM.

Table 5
The values of N and S corresponding to the most efficient PIM, SPIM and Algorithm 1, as a function of $E := -\log_{10}(e)$

E	PIM		SPIM		Alg. 1	
	N	S	N	S	N	S
1	1	4.2	1	4.2	2	4.2
2	2	3.0	2	3.0	2	4.2
3	3	2.6	2	2.9	2	4.2
4	3	2.6	2	2.5	2	2.6
5	3	1.9	3	2.5	3	2.3

5. Conclusions

In this paper we extended the scheme of Sommeijer [9], which uses extrapolation to accelerate a fixed step time integrator. The method uses similar ideas as the PIM. We analysed the linear stability properties of the method as a function of the eigenvalues of the underlying single-step integrator. We focused on the schemes based on linear and quadratic extrapolation, since for schemes that use higher order extrapolations, only a small speedup can be obtained.

Contrary to the PIM, the method based on linear extrapolation has a connected stability region, which is advantageous for problems with a large connected range of eigenvalues, such as for integrators for parabolic PDEs. The stability region of the method based on quadratic extrapolation splits into several unconnected regions. Compared to the PIM, the stability region of our scheme remains connected for a larger range of speedups. However, as the speedup becomes larger, the outer unconnected parts of the stability region shrink fast when the speedup increases. Both linear and quadratic extrapolation methods lose zero-stability as the speedup grows to infinity.

Due to the properties of the stability region, the methods are well suited for problems with a spectrum that is not limited to a small strip around the real axis, but spread out over the unit circle, as is the case for lattice-Boltzmann models. This is a topic of future research.

References

[1] V. Alexiades, G. Amiez, P. Gramaud, Super-time-stepping acceleration of explicit schemes for parabolic problems, Comm. Numer. Methods Eng. 12 (1996) 31–42.
[2] C.W. Gear, I.G. Kevrekidis, Projective methods for stiff differential equations: problems with gaps in their eigenvalue spectrum, SIAM J. Sci. Comput. 24 (4) (2003) 1091–1106.
[3] C.W. Gear, I.G. Kevrekidis, Telescopic methods for parabolic differential equations, J. Comput. Phys. 187 (1) (2003) 95–109.
[4] C.W. Gear, I.G. Kevrekidis, C. Theodoropoulos, "coarse" integration/bifurcation analysis via microscopic simulators: micro-galerkin methods, Comput. Chem. Eng. 26 (2002) 941–963.
[5] F.M. Goodman, Algebra: Abstract and Concrete (Stressing Symmetry), second ed., Prentice-Hall, Englewood Cliff, NJ, 2003.
[6] I.G. Kevrekidis, C.W. Gear, J.M. Hyman, P.G. Kevrekidis, O. Runborg, K. Theodoropoulos, Equation-free multiscale computation: enabling microscopic simulators to perform system-level tasks, Comm. Math. Sci. 1 (4) (2003) 715–762.
[7] V.I. Lebedev, Explicit difference schemes with variable time steps for solving stiff systems of equations, in: Vulkov, Wasniewski, Yalamov, (Eds.), Numerical Analysis and Its Applications, Proc. WNAA '96, Bulgaria, Springer, Berlin, 1997, 274–283.
[8] R. Rico-Martinez, C.W. Gear, I.G. Kevrekidis, Coarse projective kMC integration: forward/reverse initial and boundary value problems, J. Comput. Phys. 196 (2) (2004) 474–489.
[9] B.P. Sommeijer, Increasing the real stability boundary of explicit methods, Comput. Math. Appl. 19 (6) (1990) 37–49.
[10] J.G. Verwer, Explicit Runge–Kutta methods for parabolic partial differential equations, Appl. Numer. Math. 22 (1996) 359–379.